Support Information

Ir Doping Induced Phase Transformation and Morphological Reconstruction of MnO_2 for Efficient Alkaline Water Oxidation

Wenlan Hong, Yu Shuai, Shucheng Liu and Yi Liu*

(School of Physical Sciences, Guizhou University, Guiyang 550025, China)

Experimental Section

Materials:

Iridium(III) chloride trihydrate ($IrCl_3 \cdot 3H_2O$), potassium persulfate ($K_2S_2O_8$), manganese(II) chloride ($MnCl_2$), potassium hydroxide (KOH), and anhydrous ethanol ($C_2H_5O_5$) were purchased from Shanghai Macklin Biochemical Technology Co., Ltd. Nafion perfluorinated resin solution (5 wt.%) was purchased from Alfa Aesar (China) Chemical Co., Ltd. All reagents used in this work were of analytical grade and used without further purification.

Preparation of β-MnO_2:

503.4 mg of $MnCl_2$ and 1081 mg of $K_2S_2O_8$ were added into a polytetrafluoroethylene (PTFE) liner of a 50 mL autoclave. 20 mL of deionized water was added to the liner together with a magnetic stir bar. The liner was sealed and the mixture was stirred for 1 hour to ensure homogeneity. Subsequently, the liner was placed in the autoclave outer shell, tightened, and transferred to an oven for hydrothermal treatment at 150 °C for 24 hours. After the reaction, the black precipitate was collected by centrifugation, washed several times with anhydrous ethanol and deionized water successively, and finally dried in an oven at 80 °C for 12 hours to obtain the black solid product β-MnO_2.

Preparation of Ir-MnO_2:

The preparation procedure was the same as that for β-MnO_2, except that 74.2 mg, 156.7 mg, 248.9 mg, and 352.6 mg of $IrCl_3 \cdot 3H_2O$ were respectively added to the precursor solution to obtain the $Ir_{0.05}Mn_{0.95}O_2$, $Ir_{0.10}Mn_{0.90}O_2$, $Ir_{0.15}Mn_{0.85}O_2$, and $Ir_{0.20}Mn_{0.80}O_2$ samples.

Characterization:

The morphology and crystal plane structure of the different samples were characterized by scanning electron microscopy (SEM, HITACHI SU8010) and high-resolution transmission electron microscopy (HRTEM, FEI Talos F200X). Phase composition and structural analysis were performed by X-ray diffraction (XRD, Bruker D8 Advance) using Cu $_{K\alpha}$ radiation at a scan rate of 5° min^{-1}. The valence states of the elements in the samples were characterized by X-ray photoelectron spectroscopy

(XPS). Prior to data processing, the binding energies were calibrated using the C 1s peak at 284.8 eV. The specific surface of the samples were analyzed by BET tester (BSD-PM1, Bester Instrument Technology Co, Ltd, China). Inductively coupled plasma mass spectrometry(ICP-MS) was obtained on agilent ICPOES730.

Electrochemical measurements:

Electrochemical performance tests were carried out at room temperature using a CHI 760E electrochemical workstation in a three-electrode system. The oxygen evolution reaction (OER) was evaluated in 1 M KOH electrolyte, with a mercury/mercury oxide (Hg/HgO) electrode as the reference electrode and a platinum plate as the counter electrode. Working electrode preparation: 10 mg of catalyst was dispersed in a solution composed of 800 μL of anhydrous ethanol, 180 μL of deionized water, and 20 μL of Nafion. The mixture was then ultrasonicated for 1 hour to form a homogeneous catalyst ink. Subsequently, 5 μL of the catalyst ink was pipetted each time onto a carbon paper (with both length and width of 5 mm). After drying, another aliquot of the catalyst ink was dropped, and this process was repeated for a total of eight times, resulting in a catalyst loading of approximately 0.4 mg.Prior to the measurements, the electrode was scanned by cyclic voltammetry until stabilization, and then linear sweep voltammetry (LSV) curves were recorded at a scan rate of 5 mV s^{-1}. All potentials were converted to the reversible hydrogen electrode (RHE) scale using the following formula:

$$E(vs.RHE) = E(vs.Hg/HgO) + 0.098\ V + 0.059 \times pH\ (pH = 13.8) \quad (1)$$

The Tafel plots were obtained by fitting the polarization curves to the equation $\eta = b \log(j) + a$, where η is the overpotential, j is the current density, and b is the Tafel slope. Electrochemical impedance spectroscopy (EIS) was performed at a potential of 0.22 V (vs. RHE) with an amplitude of 5 mV over a frequency range from 1 Hz to 300 kHz. Cyclic voltammetry (CV) scans were conducted in the potential range of 0.32 to 0.37 V (vs. RHE) at scan rates from 10 to 120 mV s^{-1} to determine the electrochemical double-layer capacitance (C_{dl}).

The turnover frequency (TOF) is calculated from the equation below:

$$TOF = \frac{I}{4Fn} \quad (2)$$

Where I is the current (A) during linear sweep measurement, F is the Faraday constant (96485.3 $Cmol^{-1}$), and n is the mole number of active metals on the electrode.

AEMWE tests: 40 mg of $Ir_{0.20}Mn_{0.80}O_2$ or commercial RuO_2 catalyst was mixed with 3200 μL of anhydrous ethanol, 720 μL of deionized water, and 80 μL of Nafion solution, followed by ultrasonication for 1 hour to form a homogeneous solution. The solution was then sprayed onto a 1 cm × 1 cm nickel foam (loading of ca. 1 mg cm^{-2} for both catalysts), which was subsequently hot-pressed and used as the anode catalyst. Commercial Pt/C catalyst was loaded onto carbon paper as the cathode catalyst, and 1 M KOH was used as the electrolyte. Polarization curves were obtained by fitting the voltages measured at different current densities. Durability tests were performed by chronopotentiometry in 1 M KOH electrolyte at a temperature of 25 °C and a current density of 1 A cm^{-2}.

Theoretical calculations:

Since high-resolution transmission electron microscopy (HRTEM) revealed that the predominant exposed crystal plane of β-MnO_2 is the (110) plane, while that of $Ir_{0.20}Mn_{0.80}O_2$ is the (211) plane, different surface slabs were constructed for the calculations: the (110) surface slab model of β-MnO_2 and the (211) surface slab model of $Ir_{0.20}Mn_{0.80}O_2$. Both models consist of three layers with the same number of atoms. Specifically, the (110) slab model of β-MnO_2 contains 12 Mn atoms and 24 O atoms, while the (211) slab model of $Ir_{0.20}Mn_{0.80}O_2$ contains 10 Mn atoms, 2 Ir atoms, and 24 O atoms. Density functional theory (DFT) calculations were performed using the Vienna Ab initio Simulation Package (VASP) to analyze the free energy diagrams of the catalytic reactions for the different models[1, 2]. The projector augmented wave (PAW) method was employed to describe the ion–electron interaction, and the exchange–correlation effects were treated using the Perdew–Burke–Ernzerhof (PBE) functional within the generalized gradient approximation (GGA)[3, 4]. In the calculations, the plane-wave cutoff energy was set to 500 eV, the energy convergence criterion was 1×10^{-5} eV, and the force convergence criterion was –0.02 eV/Å. A k-point mesh of 3 × 3 × 1 was used, and a vacuum layer of approximately 15 Å was applied perpendicular to the surface to avoid interlayer interactions. The reaction free energy ΔG was determined using the computational hydrogen electrode (CHE) model, as shown in the following equation:

$$\Delta G=\Delta E+\Delta ZPE-T\Delta S \quad (3)$$

where ΔE, ΔZPE, T, and ΔS represent the change in reaction energy, zero-point energy, temperature, and change in entropy, respectively.

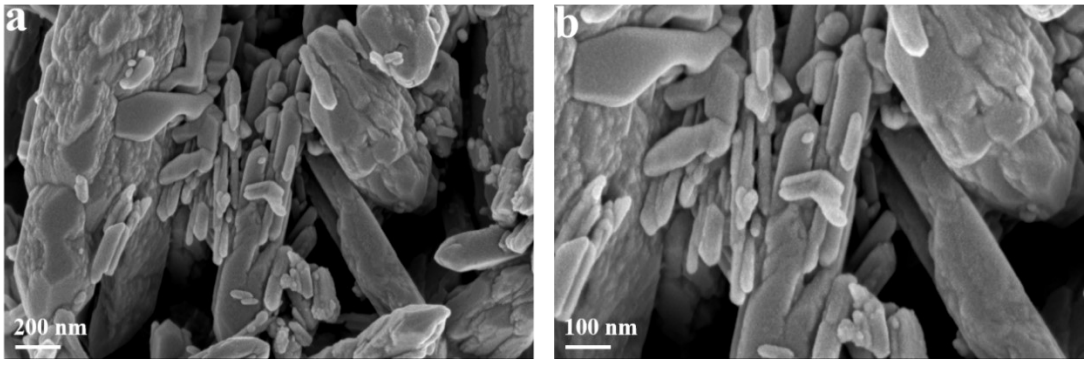

Fig.S1 The SEM images of β-MnO_2

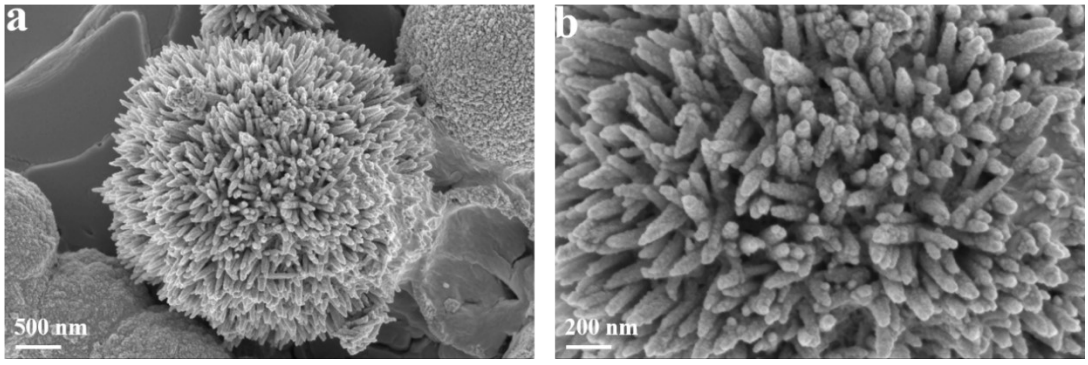

Fig.S2 The SEM images of $Ir_{0.20}Mn_{0.80}O$

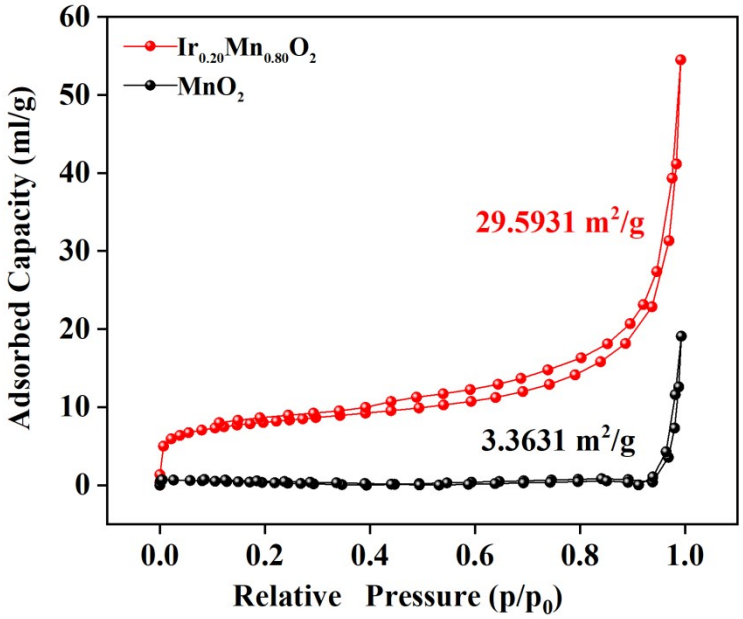

Fig.S3 Specific surface area measurement results of $Ir_{0.20}Mn_{0.80}O_2$ and MnO_2

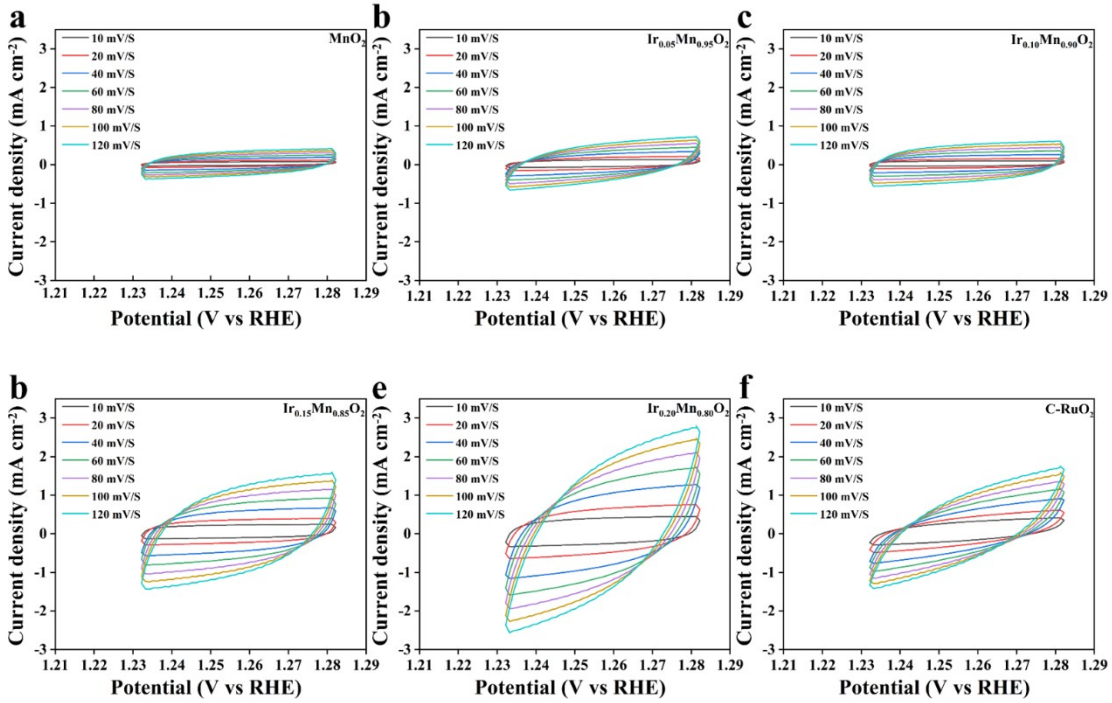

Fig.S4 The CV curves of (a) MnO_2, (b) $Ir_{0.05}Mn_{0.95}O_2$, (c))$Ir_{0.10}Mn_{0.90}O_2$, (d)$Ir_{0.15}Mn_{0.85}O_2$, (e) $Ir_{0.20}Mn_{0.80}O_2$ and (f)C- RuO_2 with different scan rates from 10 to 120 mV S^{-1}

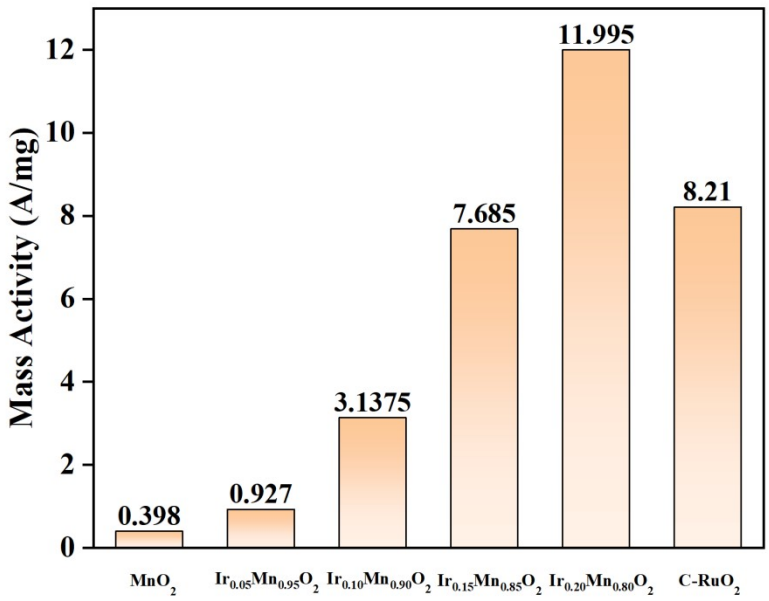

Fig.S5 Mass activities of different samples at an overpotential of η = 300 mV

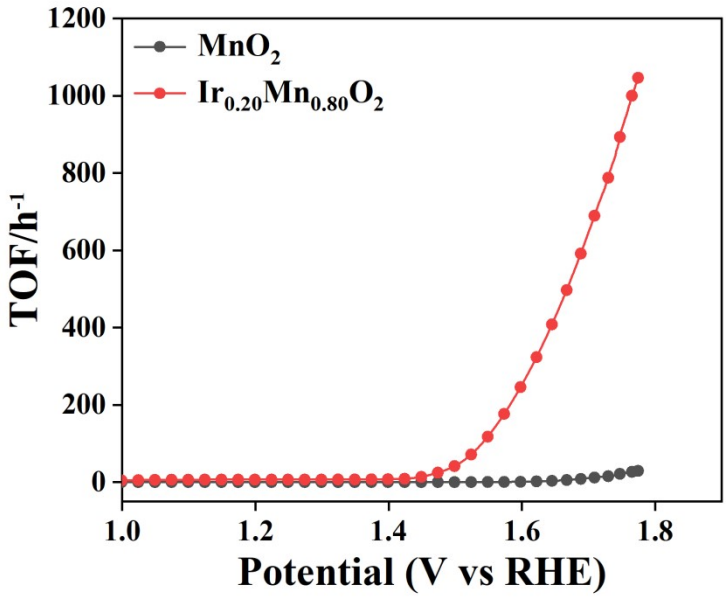

Fig.S6 TOF of $Ir_{0.20}Mn_{0.80}O_2$ and MnO_2

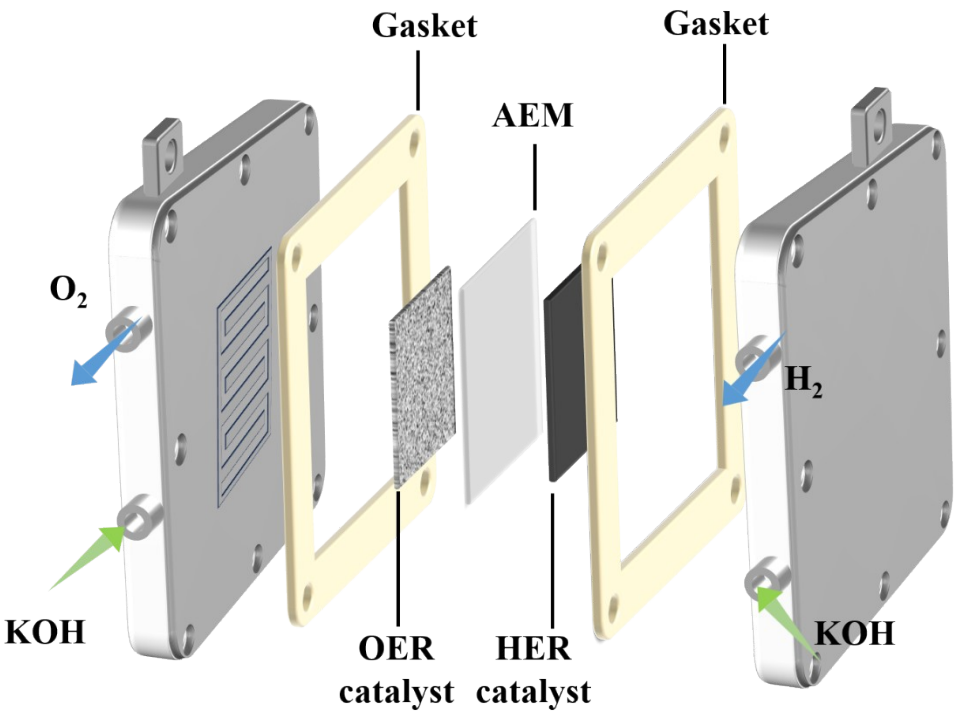

Fig.S7 Schematic diagram of the anion exchange membrane electrolyzer.

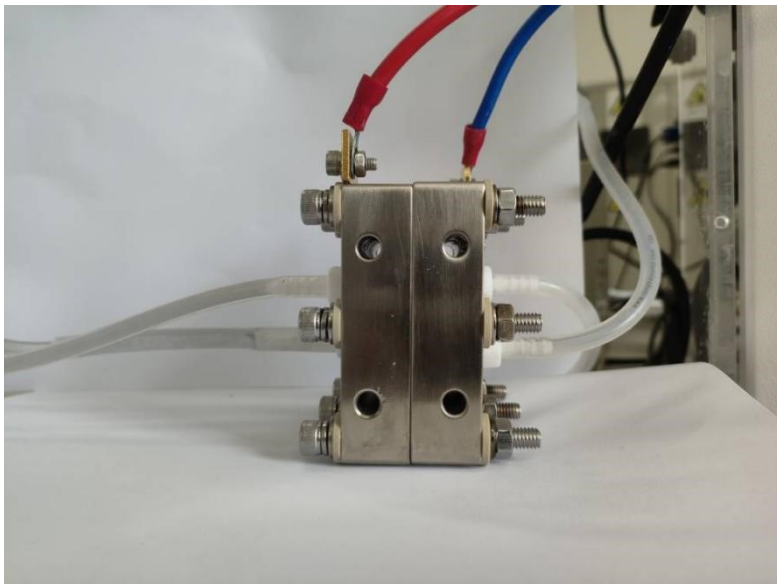

Fig.S8 Photograph of the anion exchange membrane electrolyzer

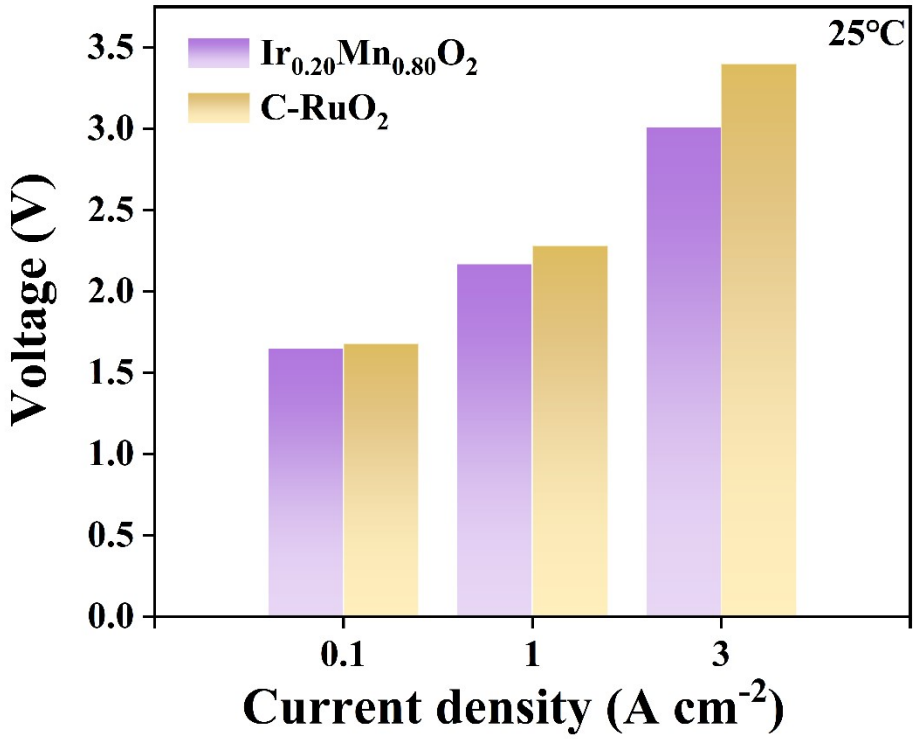

Fig.S9 The voltages of $Ir_{0.20}Mn_{0.80}O_2$ and commercial RuO_2 at different current densities

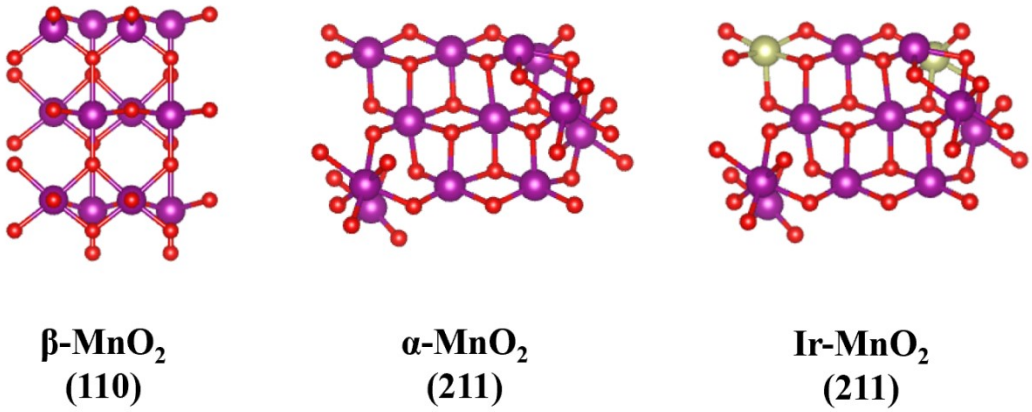

Fig.S10 Computational models of β-MnO_2 , α-MnO_2 and $Ir_{0.20}Mn_{0.80}O_2$

Table S1. ICP data of $Ir_{0.20}Mn_{0.80}O_2$

Samples	Ir(wt%)	Mn(wt%)	Ir/Mn atomic ratio
$Ir_{0.20}Mn_{0.80}O_2$	25.9656%	30.5432%	1 : 4.115
$Ir_{0.20}Mn_{0.80}O_2$	26.4588%	30.5535%	1 : 4.04
$Ir_{0.20}Mn_{0.80}O_2$	26.3912%	30.3101%	1 : 4.02

Table S2. Calculated average oxidation state (AOS) data of MnO_2 and $Ir_{0.20}Mn_{0.80}O_2$

Sample	Eb1 (eV)	Eb2 (eV)	ΔE_{3s} (ev)	AOS
MnO_2	83.49	88.01	4.52	3.9296
$Ir_{0.20}Mn_{0.80}O_2$	84.12	89.76	5.64	2.5072

Table S3. Comparison of the OER activity of $Ir_{0.20}Mn_{0.80}O_2$ with other reported electrocatalysts.

Catalyst	Electrolyte	(mV vs. RHE) @ 10mA/cm^2	Tafel slope (mV/dec)	Ref.
$Ir_{0.20}Mn_{0.80}O_2$	**1 M KOH**	**269**	**116.88**	**This work**
MnO_2-0.5IL	1 M KOH	394	49	5
β-MnO_2−Ru	1 M KOH	278	62	6
Ir-MnO_x	1 M $HClO_4$	270	51.5	7
Ir-IrαMnO_2	0.1 M $HClO_4$	268	55.71	8
Se-MnO_2	0.5 M H_2SO_4	345	64.5	9
Nd-γ-MnO_2	1 M H_2SO_4	391	88	10
Ir-Co_3O_4	0.5 M H_2SO_4	236	52.6	11
IrO_2/MnO_2	0.5 M H_2SO_4	300	32	12
$Ir_{0.4}$/$Mn_{0.6}$	0.5 M H_2SO_4	286	40	13
$Mn_{0.1}Ir_{0.9}O_2$	0.5 M H_2SO_4	269	45	14

Table S4. ICP-MS data of Mn ions in the electrolyte after stability testing of MnO_2 and $Ir_{0.20}Mn_{0.80}O_2$

Sample Name	Element	Content (μg/L)
MnO_2	Mn	1.1113
$Ir_{0.20}Mn_{0.80}O_2$	Mn	0.6799

References

1. G. Kresse and J. Furthmiiller, Efficiency of ab-initio total energy calculations for metals and semiconductors using a plane-wave basis set, *Comput. Mater. Sci.*, 1996, **15**, 10.
2. P. E. Blöchl, Projector augmented-wave method, *Phys. Rev. B*, 1994, **50**, 17953-17979.
3. G. Kresse and J. Furthmüller, Efficient iterative schemes for ab initio total-energy calculations using a plane-wave basis set, *Phys. Rev. B*, 1996, **54**, 16.
4. G. Kresse and D. Joubert, From ultrasoft pseudopotentials to the projector augmented-wave method, *Phys. Rev. B*, 1999, **59**, 3.
5. G. Yan, Y. Lian, Y. Gu, C. Yang, H. Sun, Q. Mu, Q. Li, W. Zhu, X. Zheng, M. Chen, J. Zhu, Z. Deng and Y. Peng, Phase and Morphology Transformation of MnO_2 Induced by Ionic Liquids toward Efficient Water Oxidation, *ACS Catalysis*, 2018, **8**, 10137-10147.
6. Y. Qin, Y. Liu, Y. Zhang, Y. Gu, Y. Lian, Y. Su, J. Hu, X. Zhao, Y. Peng, K. Feng, J. Zhong, M. H. Rummeli and Z. Deng, Ru-Substituted MnO_2 for Accelerated Water Oxidation: The Feedback of Strain-Induced and Polymorph-Dependent Structural Changes to the Catalytic Activity and Mechanism, *ACS Catalysis*, 2022, **13**, 256-266.
7. L. Quan, Y. Cao, J. Liu, B. Y. Xia, X. Zhao and B. You, Wrinkled Ir-MnOx nanospheres as pH-universal electrocatalysts for oxygen evolution reaction, *Journal of Materials Chemistry A*, 2024, **12**, 19958-19967.
8. X. Teng, K. Zhang, Z. Yang, H. Zhao, J. Yun and J. Zhang, Surface atomic step iridium nanocrystals on αMnO_2 enhance oxygen evolution reaction performance, *Electrochimica Acta*, 2026, **549**, 148065.
9. S. Pan, S. Wang, Z. Xie, H. Li, Y. Fu and D. Wang, Se-doped MnO_2 as a low-cost and high-efficiency catalyst for acidic oxygen evolution reaction, *Nano Research*, 2025, **18**, 94907912.
10. Q. Hu, A. Li, Y. Sun, L. Liu, T. Liu, C. Li and H. Han, Tailor Control of Neodymium Doping Sites in γ-MnO_2 for Stable Oxygen Evolution Reaction in Acidic Electrolyte, *Advanced Functional Materials*, 2025, **36**,2423709.
11. Y. Zhu, J. Wang, T. Koketsu, M. Kroschel, J.-M. Chen, S.-Y. Hsu, G. Henkelman, Z. Hu, P. Strasser and J. Ma, Iridium single atoms incorporated in Co_3O_4 efficiently catalyze the oxygen evolution in acidic conditions, *Nature Communications*, 2022, **13**,7754.
12. F. Wang, J. Sui, Z. Wang, S. Ling, W. Zhang, Y. Yan, J. Qi and X. Luo, IrO_2/MnO_2 metal oxide-support interaction enables robust acidic water oxidation, *Journal of Colloid and Interface Science*, 2025, **683**, 160-169.
13. Z. Zhou, W. Q. Zaman, W. Sun, L.-m. Cao, M. Tariq and J. Yang, Cultivating crystal lattice distortion in IrO_2 via coupling with MnO_2 to boost the oxygen evolution reaction with high intrinsic activity, *Chemical Communications*, 2018, **54**, 4959-4962.
14. H. Gao, C. Song, R. Chen, T. Wu, J. Zou, S. Du, C.-L. Dong, Y.-C. Huang, R. Zhu, Y. Wang and S. Wang, Activation of iridium site based on IrO_2 catalysts

towards highly stable PEM water electrolyzer, *Chemical Engineering Science*, 2025, **302**,120912.